

## Electronic Supplementary Information

### Transfection-capable polycationic nanovectors which include PEGylated-cyclodextrin structural units. A new synthesis pathway.

A. I. Dascalu,<sup>a</sup> R. Ardeleanu,<sup>a</sup> A. Neamtu,<sup>a,b</sup> S. S. Maier,<sup>c,a</sup> C. M. Uritu,<sup>a</sup> A. Nicolescu,<sup>a</sup> M. Silion,<sup>a</sup>  
D. Peptanariu,<sup>a</sup> M. Calin,<sup>d</sup> M. Pinteala,<sup>a,\*</sup>

<sup>a</sup> Centre of Advanced Research in Bionanoconjugates and Biopolymers, “Petru Poni” Institute of Macromolecular Chemistry, 700487 Iasi, Romania,

<sup>b</sup> Regional Institute of Oncology (IRO), TRANSCEND Research Center, str. General Henry Mathias Berthlot nr. 2-4, Iasi, Romania,

<sup>c</sup> “Gheorghe Asachi” Technical University of Iasi, 700050 Iasi, Romania

<sup>d</sup> “Nicolae Simionescu” Institute of Cellular Biology and Pathology, Bucharest, 050568, Romania

Email: Mariana Pinteala\*: pinteala@icmpp.ro;

\* Corresponding author

#### Table of contents

<b>Figure S1.</b> The general synthesis pathway of acrylated $\beta$ -CD	p. 3
<b>Figure S2.</b> FTIR spectra of $\beta$ -CD-PEG-PEI conjugate and its precursors	p. 3
<b>Figure S3.</b> $^1\text{H}$ -NMR spectra of native $\beta$ -CD and of acrylated $\beta$ -CD, recorded in DMSO-d6	p. 4
<b>Figure S4.</b> $^1\text{H}$ , $^{13}\text{C}$ -HSQC spectrum of the acrylated $\beta$ -CD, recorded in DMSO-d6	p. 4
<b>Figure S5.</b> $^{13}\text{C}$ -NMR spectra of native $\beta$ -CD and of acrylated $\beta$ -CD, recorded in DMSO-d6	p. 5
<b>Figure S6.</b> XPS high-resolution spectra of C 1s (A) and O 1s (B) in the acrylated $\beta$ -CD, and of C 1s (C) and N 1s (D) in $\beta$ -CD-PEG-PEI.	p. 6
<b>Figure S7.</b> The mass spectrum of $\beta$ -CD in methanol-water solution (9:1 v/v).	p. 6
<b>Figure S8.</b> The mass spectrum of acrylated $\beta$ -CD in methanol-water solution (9:1 v/v)	p. 7
<b>Figure S9.</b> $^1\text{H}$ -NMR spectrum of $\beta$ -CD-PEG-PEI, recorded in $\text{D}_2\text{O}$	p. 7
<b>Figure S10.</b> $^1\text{H}$ , $^{13}\text{C}$ -HMBC spectrum of the $\beta$ -CD-PEG-PEI conjugate, recorded in $\text{D}_2\text{O}$	p. 8
<b>Figure S11.</b> $^{13}\text{C}$ -NMR spectrum of $\beta$ -CD-PEG-PEI conjugate, recorded in $\text{D}_2\text{O}$	p. 8

<b>Figure S12.</b> Mass spectra of $\beta$ -CD-PEG-PEI in methanol-water solutions 9:1 (v/v)	p. 9
<b>Figure S13.</b> Wide XPS scans of $\beta$ -CD-PEG-PEI conjugate. Inserted table shows theoretical and experimental values determined by XPS of the atomic compositions related to $\beta$ -CD-PEG-PEI	p. 9
<b>Figure S14.</b> Gel retardation assay of $\beta$ -CD-PEG-PEI/pLuc (A) and PEI (2 kDa)/pLuc (B) polyplexes having N/P ratios of 0, 1, 3, 5, 10, 15, and 20. Empty wells were maintained between the loaded ones to prevent artifacts	p. 10
<b>Figure S15.</b> The dependence of the zeta potential of $\beta$ -CD-PEG-PEI/pLuc polyplexes on the N/P ratios in aqueous milieu, at pH values of 7.4 and 5.5	p. 10
<b>Figure S16.</b> Molecular structure and protonation states for the PEI molecule used in theoretical modeling	p. 11
<b>Figure S17.</b> Snapshots of the initial configuration (above) and a representative conformation (below) at 7 ns for a single $\beta$ -CD-PEG-PEI molecule interacting in an “edge-on” orientation with a 60 bp dsDNA fragment (simulation 1V/DNA)	p. 11
<b>Figure S18.</b> Snapshots of the initial configuration (above) and a representative conformation (below) at 3 ns showing the DNA bending and $\beta$ -CD- PEG-PEI “adaptation” to a 96 bp DNA fragment (simulation 4V/DNA)	p. 12
<b>Figure S19.</b> The spire approximate diameter in the initial configurations (left) and at the end of simulations (right). The distances were measured between the diametrically opposed outer phosphorus atoms	p. 12
<b>Figure S20.</b> Structural parameters of the $\beta$ -CD-PEG-PEI/dsDNA complexes during simulations: (A) the RMSD of the entire DNA fragment (red) and of each spire separately (green and blue); (B) the number of hydrogen bonds formed between $\beta$ -CD-PEG-PEI and dsDNA; green and blue curves shows the H-bond number formed between individual $\beta$ -CD-PEG-PEI molecules and their corresponding dsDNA spires	p. 13
<b>Table S1.</b> Details on the four systems simulated in this study	p. 13
<b>Supplementary Computational Methods</b>	p. 13
<b>Supplementary References</b>	p. 15

**Figure S1.** The general synthesis pathway of acrylated  $\beta$ -CD.

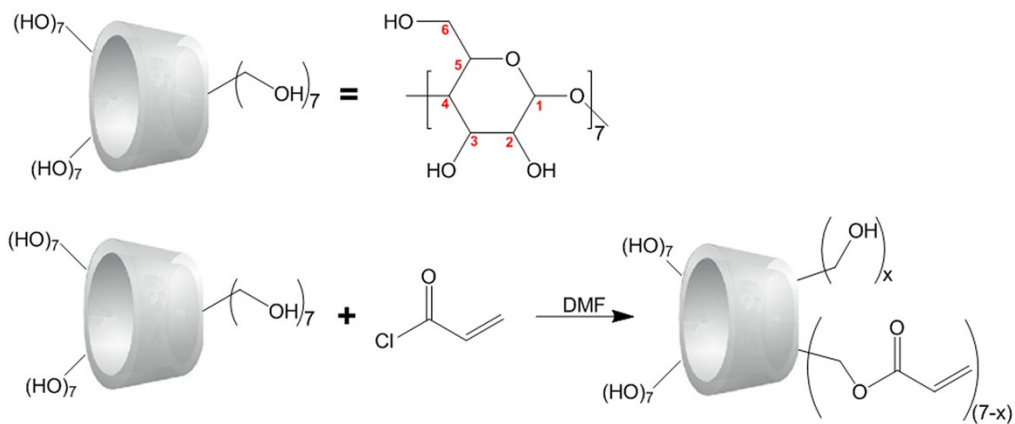


**Figure S2.** FTIR spectra of  $\beta$ -CD-PEG-PEI conjugate and its precursors.

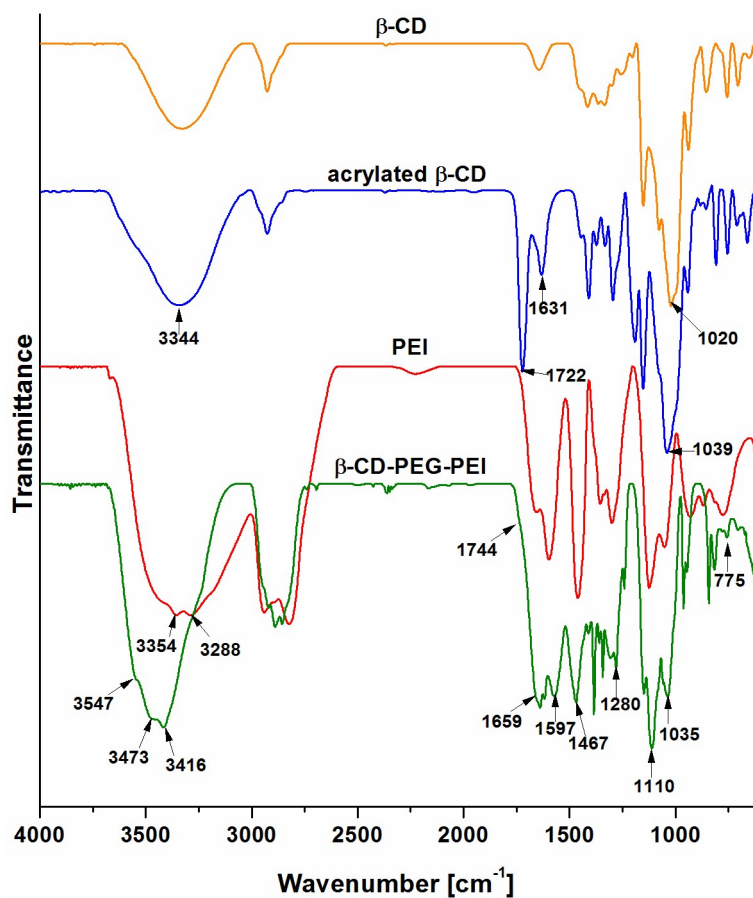


**Figure S3.**  $^1\text{H}$ -NMR spectra of native  $\beta$ -CD (bottom) and of acrylated  $\beta$ -CD (top). Both spectra are recorded in DMSO- $d_6$ .

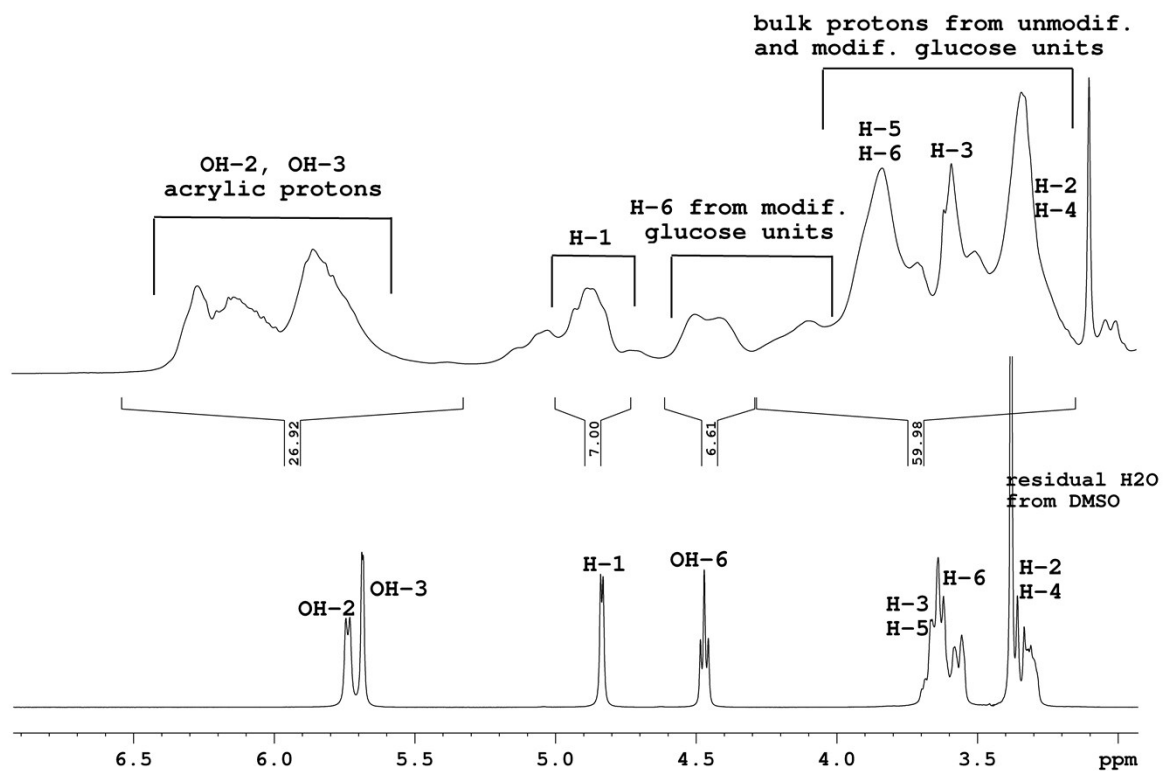


**Figure S4.**  $^1\text{H}$ ,  $^{13}\text{C}$ -HSQC spectrum of the acrylated  $\beta$ -CD, recorded in DMSO- $d_6$ .

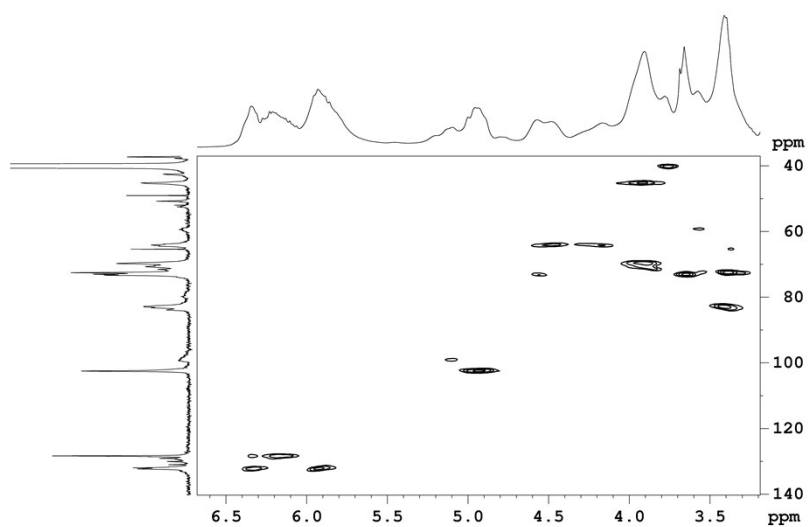


**Figure S5.**  $^{13}\text{C}$ -NMR spectra of native  $\beta$ -CD (bottom) and of acrylated  $\beta$ -CD (top), recorded in DMSO- $d_6$ . The signals annotated with C-6' are the  $\text{CH}_2\text{-O}$  groups from modified glucose units and with C-6'' are the  $\text{CH}_2\text{-O}$  groups from unmodified glucose units.

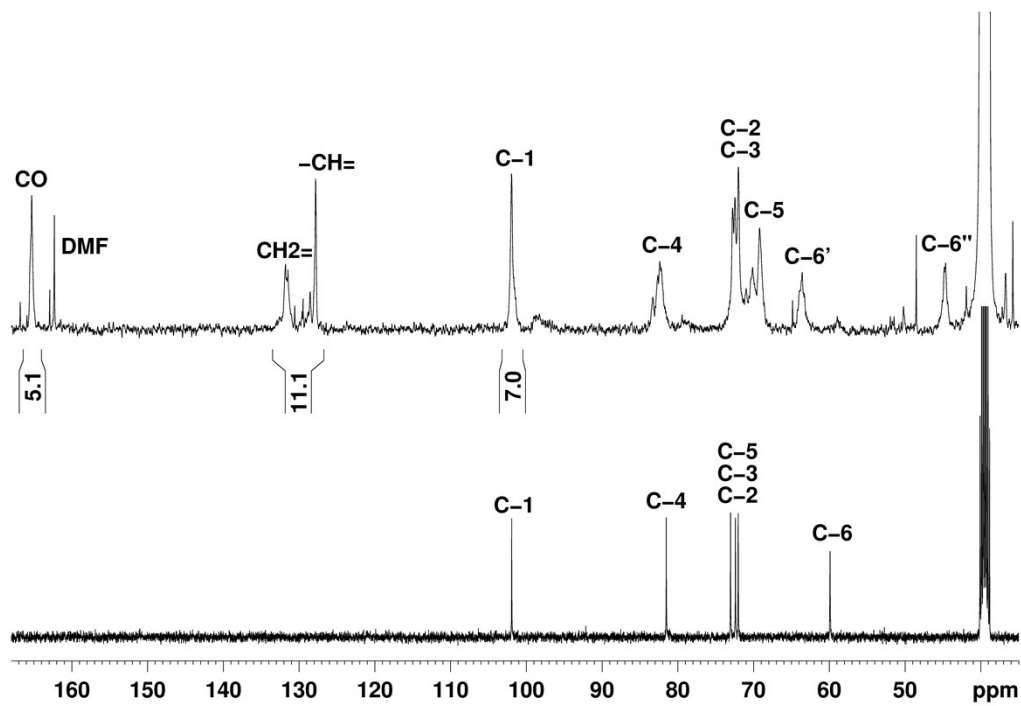


**Figure S6.** XPS high-resolution spectra of C 1s (A) and O 1s (B) in the acrylated  $\beta$ -CD, and of C 1s (C) and N 1s (D) in  $\beta$ -CD-PEG-PEI. Samples were examined in dried-powder state.

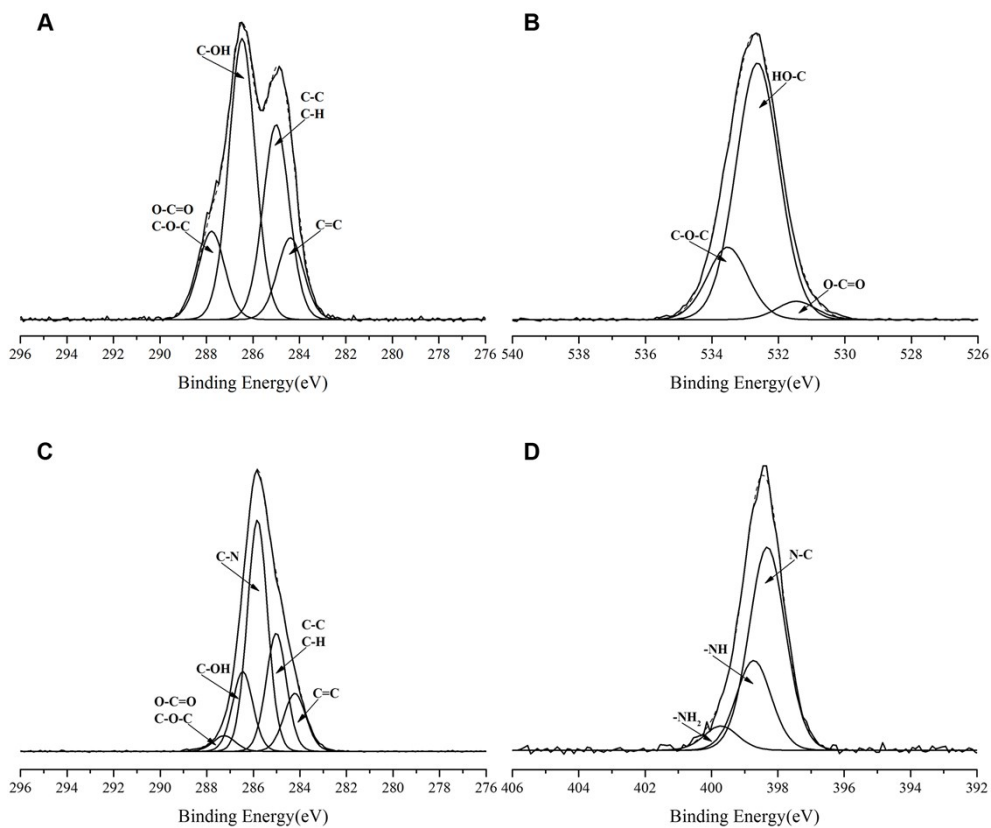


**Figure S7.** The mass spectrum of  $\beta$ -CD in methanol-water solution (9:1 v/v).

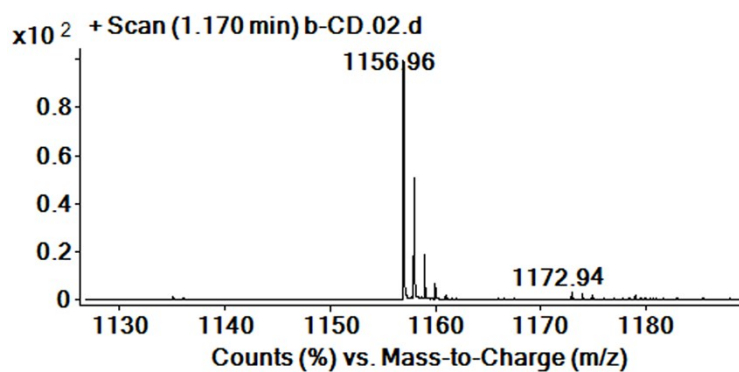


**Figure S8.** The mass spectrum of acrylated  $\beta$ -CD in methanol-water solution 9:1 (v/v).

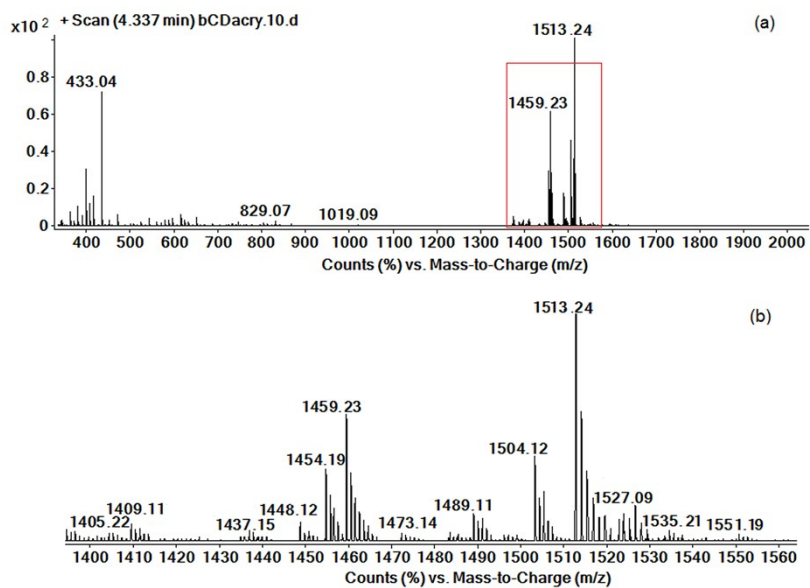


**Figure S9.**  $^1\text{H-NMR}$  spectrum of  $\beta$ -CD-PEG-PEI, recorded in  $\text{D}_2\text{O}$ .

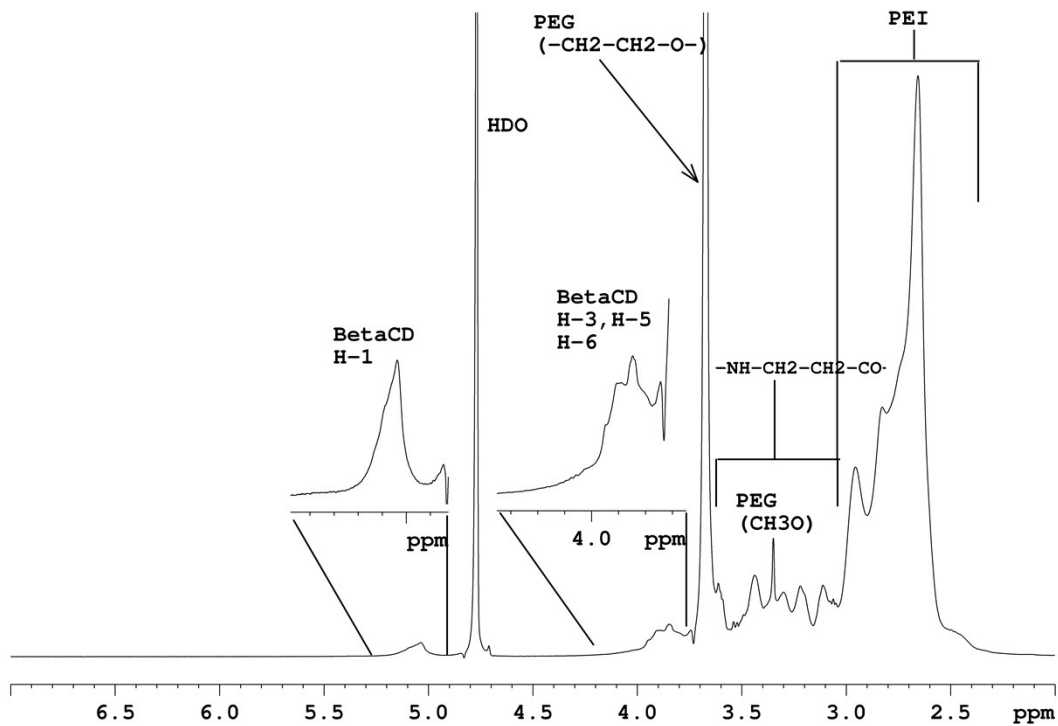


**Figure S10:**  $^1\text{H}, ^{13}\text{C}$ -HMBC spectrum of the  $\beta$ -CD-PEG-PEI conjugate, recorded in  $\text{D}_2\text{O}$ .

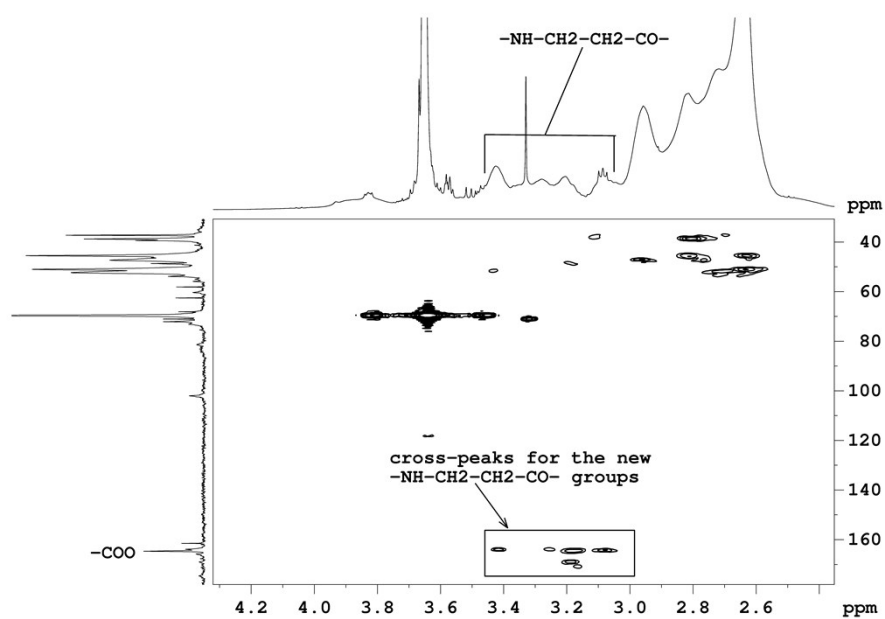


**Figure S11.**  $^{13}\text{C}$ -NMR spectrum of  $\beta$ -CD-PEG-PEI conjugate recorded in  $\text{D}_2\text{O}$ .

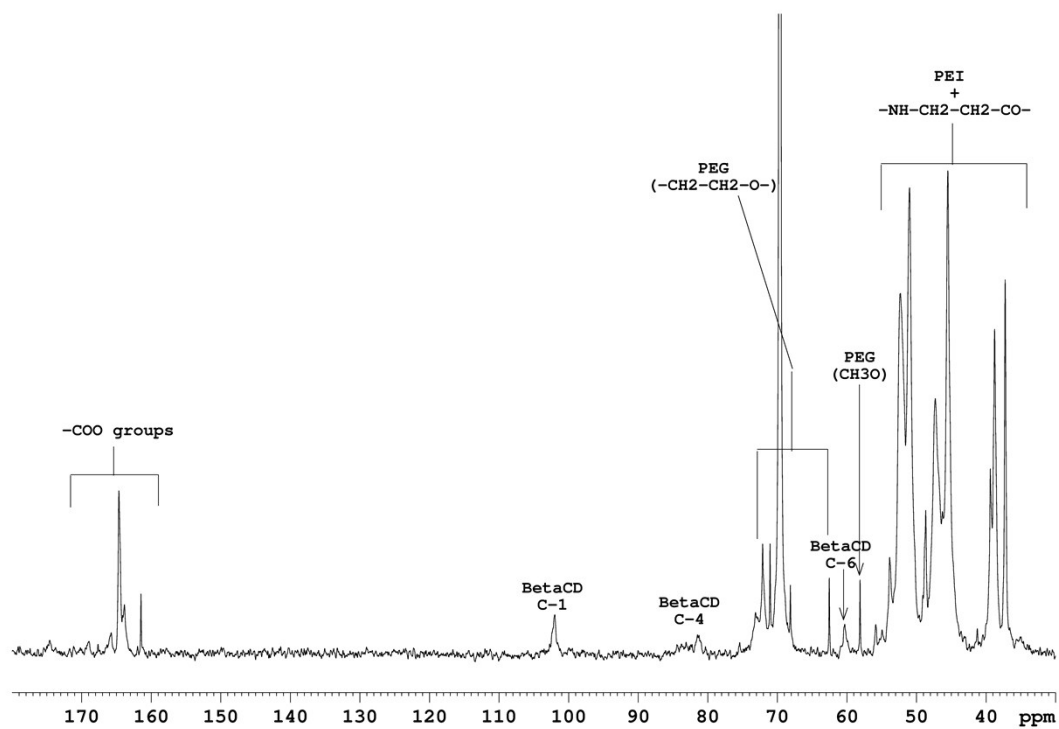


**Figure S12.** Mass spectra of  $\beta$ -CD-PEG-PEI in methanol-water solutions 9:1 (v/v)

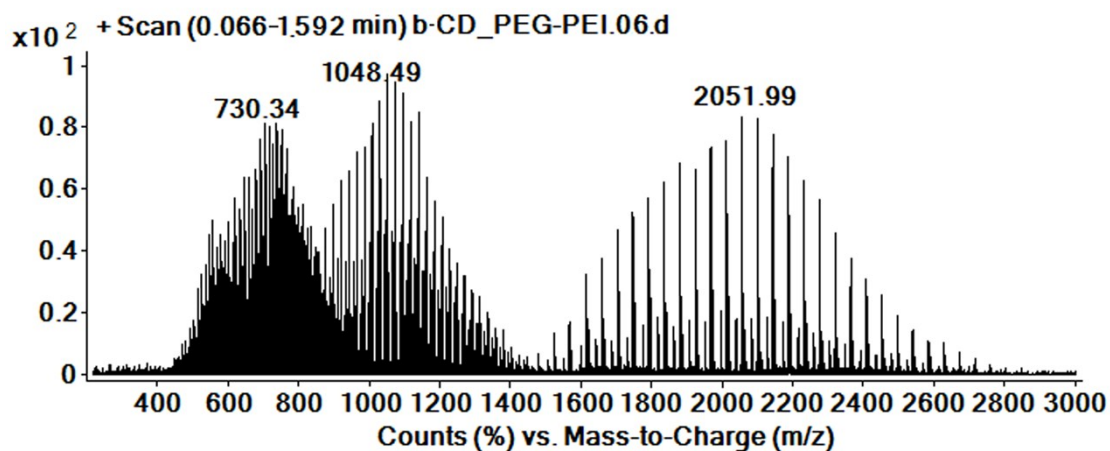
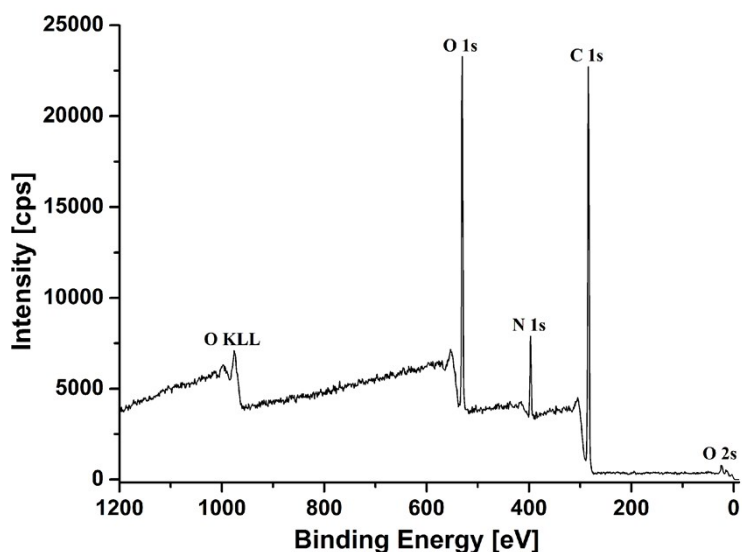


**Figure S13.** Wide XPS scans of  $\beta$ -CD-PEG-PEI conjugate. Inserted table shows theoretical and experimental values determined by XPS of the atomic compositions related to  $\beta$ -CD-PEG-PEI.



Carrier type	Theoretical Atomic Concentration of Element (%)		
	C	N	O
$\beta$ -CD with 7 acrylic groups	60.00	-	40.00
PEG-amine	66.67	1.06	31.37
PEI 2 kDa	64.62	35.38	
$\beta$ -CD-PEG-PEI with 6 PEI and 1 PEG-amine	64.21	29.59	6.20
	Experimental Atomic Concentration of Element (%), determined by XPS		
Synthesized $\beta$ -CD-PEG-PEI	65.68	28.32	6.00

**Figure S14:** Gel retardation assay of  $\beta$ -CD-PEG-PEI/pLuc (A) and PEI (2 kDa)/pLuc (B) polyplexes having N/P ratios of 0, 1, 3, 5, 10, 15, and 20. Empty wells were maintained between the loaded ones to prevent artifacts.

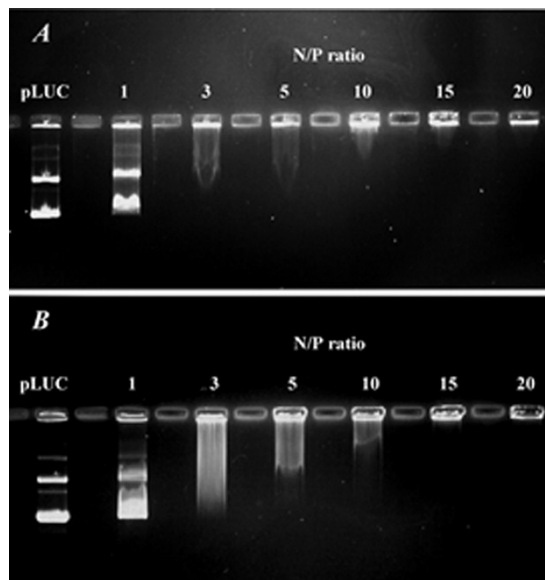


**Figure S15.** The dependence of the zeta potential of  $\beta$ -CD-PEG-PEI/pLuc polyplexes on different N/P ratios in aqueous milieu, at pH values of 7.4 and 5.5.

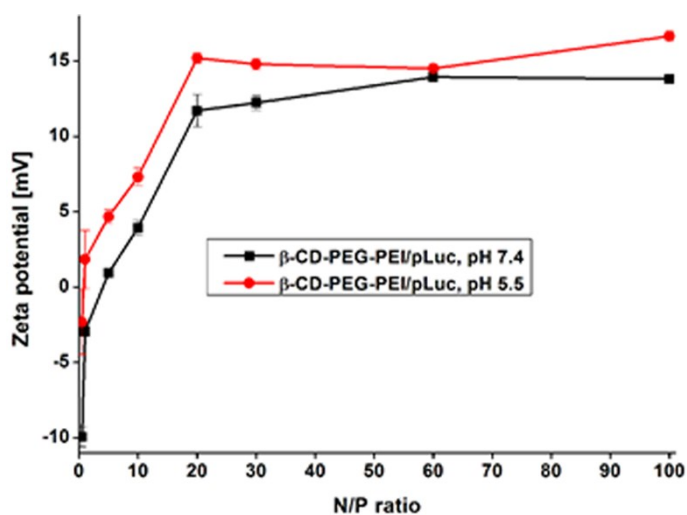


**Figure S16.** Molecular structure and protonation states for the PEI molecule used in theoretical modeling.

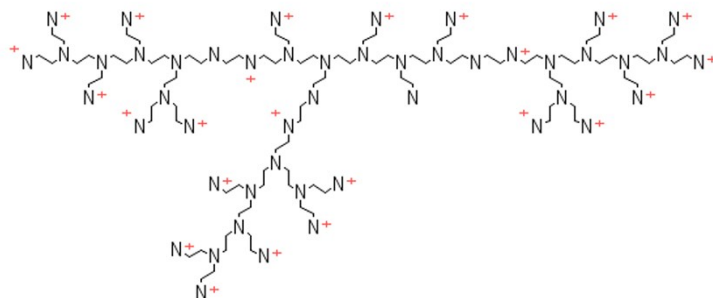


**Figure S17.** Snapshots of the initial configuration (above) and a representative conformation (below) at 7 ns for a single  $\beta$ -CD-PEG-PEI molecule interacting in an “edge-on” orientation with a 60 bp dsDNA fragment (simulation 1C/DNA).

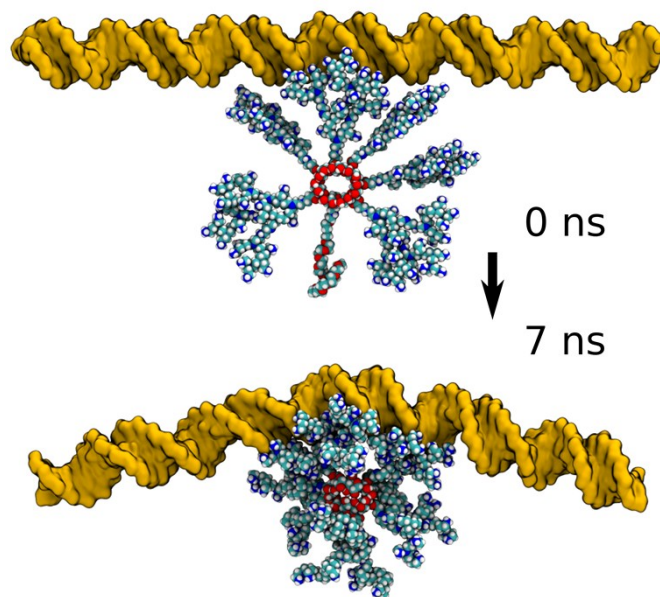


**Figure S18.** Snapshots of the initial configuration (above) and a representative conformation (below) at 3 ns showing the DNA bending and  $\beta$ -CD-PEG-PEI “adaptation” to a 96 bp DNA fragment (simulation 4C/DNA).

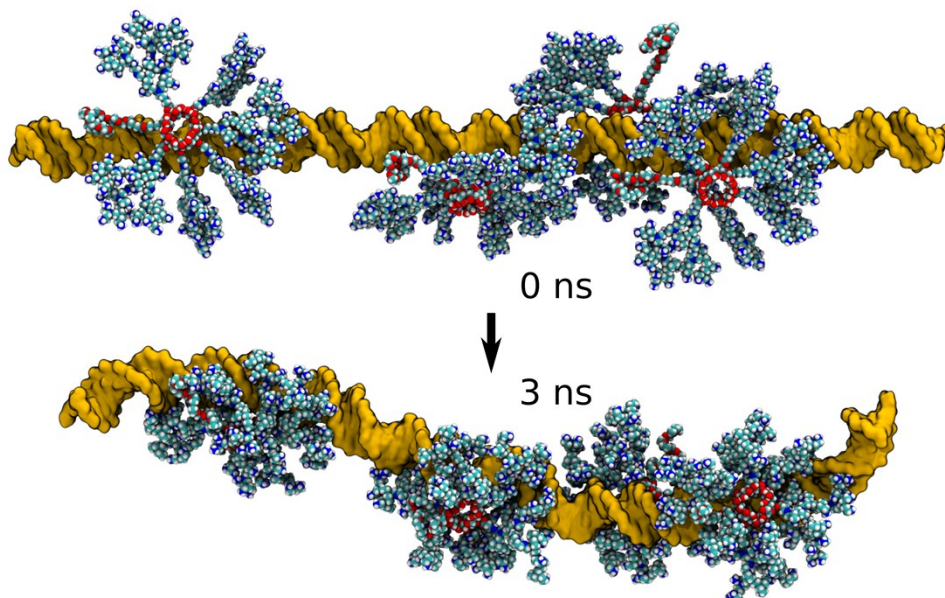


**Figure S19.** The spire approximate diameter in the initial configurations (left) and at the end of simulations (right). The distances were measured between the diametrically opposed outer phosphorus atoms.

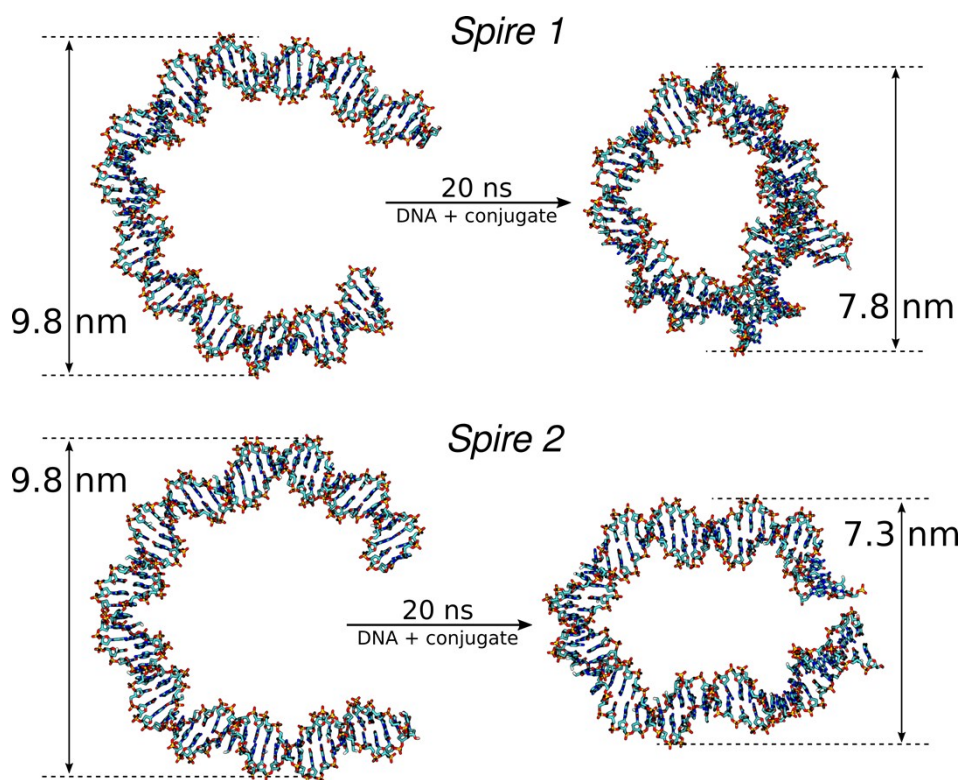


**Figure S20.** Structural parameters of the  $\beta$ -CD-PEG-PEI/dsDNA complexes during simulations: (A) the RMSD of the entire DNA fragment (red) and of each spire separately (green and blue); (B) the number of hydrogen bonds formed between  $\beta$ -CD-PEG-PEI and dsDNA; green and blue curves shows the H-bond number formed between individual  $\beta$ -CD-PEG-PEI molecules and their corresponding dsDNA spires.

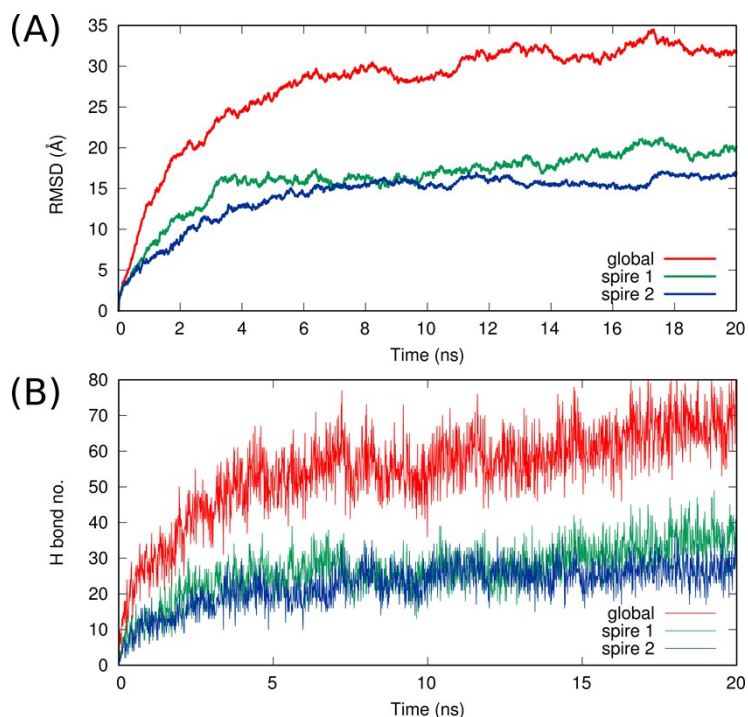


**Table S1.** Details on the four systems simulated in this study.

Simulation code	DNA	$\beta$ -CD-PEG-PEI	H <sub>2</sub> O molec.	Ions	No. of atoms	MD length (ns)
1C/DNA	60 bp	1	85734	225 Na <sup>+</sup> ; 249 Cl <sup>-</sup>	264214	10
4C/DNA	96 bp	4	176327	262 Na <sup>+</sup> ; 644 Cl <sup>-</sup>	546945	10
2C/DNAS	146 bp	2	168010	472 Na <sup>+</sup> ; 470 Cl <sup>-</sup>	519720	20
DNAS	146 bp	-	96096	445 Na <sup>+</sup> ; 155 Cl <sup>-</sup>	298172	20

## Supplementary Computational Methods

### Section 1. Computational methods applied for the estimation of $\beta$ -CD-PEG-PEI/pLuc volume

The volume of the equilibrated  $\beta$ -CD-PEG-PEI molecular model was calculated as the volume enclosed by the molecular surface (contact + re-entrant) constructed using the YASARA<sup>1</sup> software, giving a result of  $V_R = 37.8 \text{ nm}^3$ . For the plasmid volume estimation, a double length Dickerson-

Drew DNA dodecamer 2 X d[CGCGAATTCGCG]<sub>2</sub> double helix chain was constructed and its volume computed as above. From this volume we could calculate per base pair DNA volume (0.4703 nm<sup>3</sup>) and multiplied it with the plasmid length (5991 bp) obtaining for the total plasmid volume a value of  $V_P = 0.4703 \times 5991 = 2817.6 \text{ nm}^3$ . Further, from the N/P ratio of 80 (maximum transfection efficiency), one could calculate the number of  $\beta$ -CD-PEG-PEI corresponding to one plasmid and thus allowed us to estimate the volume of the  $\beta$ -CD-PEG-PEI/pLuc of  $V_C = 125811 \text{ nm}^3$ . This corresponds to a mean diameter  $d_C = 62 \text{ nm}$ .

## **Section 2. Computational methods to determine the compactness and stability of the nanoparticulate aggregates formed by the condensation of dsDNA by $\beta$ -CD-PEG-PEI conjugate**

### **Models construction**

A model of hyperbranched PEI (M=2000) was manually constructed and optimized using the Avogadro software.<sup>2</sup> The protonation states of the amino groups were adjusted to give an overall protonation of 50%<sup>3</sup> with a net charge of 24 per PEI molecule (Supplementary Figure 16). Similarly, a 0.75 kDa PEG-amine molecule was manually constructed and optimized using the Avogadro software. Then, a  $\beta$ -cyclodextrin molecule was substituted with 6 PEI molecules and one PEG-amine at carbon atoms in position 6, bearing a total charge of +144 elementary charges.

DNA fragments were obtained as follows. For simulations 1V/DNA and 4V/DNA (Supplementary Table 1) 5 and 8 repeats, respectively of the Dickerson-Drew dodecamer d(CGCGAATTCGCG)<sub>2</sub> were built as linear B-DNA fragments using the Maestro simulation environment.<sup>4</sup> Each Dickerson-Drew segment carried a total charge of -24 in the fully deprotonated state. For simulations 2V/DNAS and DNAS the DNA double spire (146 bp) was extracted from the Protein Data Bank (PDB) entry 1AOI<sup>5</sup> carrying a total charge of -146.

### **Simulated systems and procedures**

Compositions of the simulated systems are shown in Supplementary Table 1. For simulations 1V/DNA and 4V/DNA one and four  $\beta$ -CD-PEI/PEG molecules respectively were placed in the vicinity of the DNA fragments in an “edge-on” for 1V/DNA and “face-on” for 4V/DNA orientations. For 2V/DNAS simulation two  $\beta$ -CD-PEI/PEG molecules were manually inserted inside the two spires of nucleosomal DNA in such a way that no overlaps occurred. The configurations were then solvated and neutralized to a physiological ion concentration of 0.9%. After an initial optimization protocol including energy minimization and simulated annealing

adjustment of solvent molecules, the models were subjected to molecular dynamics (MD) production simulations. All simulations were performed using the Yasara software.<sup>6</sup> All models were described using YAMBER3 force field as implemented in Yasara-2016. TIP3P<sup>7</sup> model was used for water. The systems were simulated in the NPT ensemble using the Berendsen thermostat and barostat at 25°C and 1 atm. The MD trajectories analysis was performed using the GROMACS 4.6 molecular simulation package<sup>8</sup> and Visual Molecular Dynamics (VMD 1.9.2).<sup>9</sup>

## SUPPLEMENTARY REFERENCES

- (1) Krieger, E.; Vriend, G. YASARA View - molecular graphics for all devices - from smartphones to workstations. *Bioinformatics* **2014**, 30(20), 2981–2982.
- (2) Hanwell, M. D.; Curtis, D. E.; Lonie, D. C.; Vandermeersch, T.; Zurek, E.; Hutchison, G. R. Avogadro: an advanced semantic chemical editor, visualization, and analysis platform. *J Cheminform* **2012**, 4, 1–17.
- (3) Sun, C.; Tang, T.; Uludağ, H.; Cuervo, J. E. Molecular dynamics simulations of DNA/PEI complexes: effect of PEI branching and protonation state. *Biophys. J.* **2011**, 100(11), 2754-2763.
- (4) Schrödinger, LLC, New York, NY, 2016.
- (5) Luger, K.; Mäder, A. W.; Richmond, R. K.; Sargent, D. F., Richmond, T. J. Crystal structure of the nucleosome core particle at 2.8 Å resolution. *Nature* **1997**, 389(6648), 251–260.
- (6) Krieger, E.; Koraimann, G.; Vriend, G. Increasing the precision of comparative models with YASARA NOVA - a self-parameterizing force field. *Proteins* **2002**, 47(3), 393–402.
- (7) Jorgensen, W. L.; Chandrasekhar, J.; Madura, J. D.; Impey, R. W.; Klein, M. L. Comparison of simple potential functions for simulating liquid water. *J. Chem. Phys* **1983**, 79(2), 926–935.
- (8) Abraham, M. J.; Murtola, T.; Schulz, R.; Páll, S.; Smith, J. C.; Hess, B.; Lindahl, E. ROMACS: High performance molecular simulations through multi-level parallelism from laptops to supercomputers. *SoftwareX* **2015**, 1-2, 19–25.
- (9) Humphrey, W.; Dalke, A.; Schulten, K. VMD - Visual Molecular Dynamics. *J. Mol. Graph.* **1996**, 33–38.